



Angular dependence of strong field sequential double ionization for neon and acetylene simulated with time-dependent configuration interaction using CIS and CISD-IP

Cite as: J. Chem. Phys. **152**, 064106 (2020); <https://doi.org/10.1063/1.5133659>

Submitted: 24 October 2019 . Accepted: 19 January 2020 . Published Online: 11 February 2020

Mi Kyung Lee , Wen Li, and H. Bernhard Schlegel 

COLLECTIONS

Paper published as part of the special topic on [Ultrafast molecular sciences by femtosecond photons and electrons](#)

Note: This paper is part of the JCP Special Topic on Ultrafast Molecular Sciences by Femtosecond Photons and Electrons.



View Online



Export Citation



CrossMark

ARTICLES YOU MAY BE INTERESTED IN

[The density matrix renormalization group in chemistry and molecular physics: Recent developments and new challenges](#)

The Journal of Chemical Physics **152**, 040903 (2020); <https://doi.org/10.1063/1.5129672>

[Efficient and stochastic multireference perturbation theory for large active spaces within a full configuration interaction quantum Monte Carlo framework](#)

The Journal of Chemical Physics **152**, 054101 (2020); <https://doi.org/10.1063/1.5140086>

[Quantum mechanical/molecular mechanical trajectory surface hopping molecular dynamics simulation by spin-flip time-dependent density functional theory](#)

The Journal of Chemical Physics **152**, 024119 (2020); <https://doi.org/10.1063/1.5132879>

Lock-in Amplifiers
Find out more today



 Zurich
Instruments

Angular dependence of strong field sequential double ionization for neon and acetylene simulated with time-dependent configuration interaction using CIS and CISD-IP

Cite as: J. Chem. Phys. 152, 064106 (2020); doi: 10.1063/1.5133659

Submitted: 24 October 2019 • Accepted: 19 January 2020 •

Published Online: 11 February 2020



View Online



Export Citation



CrossMark

Mi Kyung Lee,  Wen Li, and H. Bernhard Schlegel^{a)} 

AFFILIATIONS

Department of Chemistry, Wayne State University, Detroit, Michigan 48202, USA

Note: This paper is part of the JCP Special Topic on Ultrafast Molecular Sciences by Femtosecond Photons and Electrons.

^{a)} Author to whom correspondence should be addressed: hbs@chem.wayne.edu

ABSTRACT

Strong field ionization is fundamentally important for attosecond spectroscopy and coherence control. However, the modeling beyond the single active electron approximation is still difficult. Time-dependent configuration interaction with singly excited configurations and a complex absorbing potential (TDCIS-CAP), can be used to simulate single and double ionization by intense laser fields. When the monocation does not have degenerate states, TDCIS-CAP starting from a Hartree–Fock calculation of the cation is suitable for simulating the second ionization step. When the monocation has two or more degenerate states, the simulations should treat these degenerate states equivalently. CISD-IP (single and double excitation configuration interaction with ionization) can be used to treat degenerate states of the cation on an equal footing by representing the cation wavefunctions with ionizing single (1 hole) and double (2 holes/1 particle) excitations from the neutral molecule. Since CISD-IP includes single excitations for each of the monocation states, time dependent CISD-IP with a complex absorbing potential (TDCISDIP-CAP) can also be used to simulate ionization to the dications states. In this work, TDCIS-CAP and TDCISDIP-CAP have been used to simulate the angular dependence of ionization of the neon cation and acetylene cation. In both cases, the second electron is ionized predominantly from an orbital perpendicular to the orbital involved in the first ionization. The TDCISDIP-CAP simulations show some features involving interactions between the monocation states that are not seen in the TDCIS-CAP simulations.

Published under license by AIP Publishing. <https://doi.org/10.1063/1.5133659>

I. INTRODUCTION

Double ionization by strong laser fields and the correlated nature of the two-electron ejections have attracted much attention in the past two decades. These processes can be roughly categorized as sequential (SDI) and nonsequential (NSDI) depending on whether electron recollision plays a role.^{1–3} However, such a delineation becomes problematic when the time of electron ejection becomes increasingly shorter toward less than 1 fsec. In such a process, the inherent electron correlation in the absence of electron recollision becomes important and should be treated explicitly. Therefore, modeling beyond the

single active electron (SAE) approximation is critical for understanding multielectron effect in strong field double ionization of atomic and molecular systems. The recent experimental results suggest that ionization delays as short as 500 as can be accessed using the two-electron angular streaking method, in which the angle-dependent ionization rates were measured for both electrons to extract the time-resolved dynamics.^{4,5} However, it is still difficult to extract electron correlation in this process with conventional methods.

To model such dynamics, the angular dependence of strong field single ionization has been simulated with *rt-TDDFT*^{6–8} and TDCI approaches.^{4,5,9–17} The former uses the time-dependent

Kohn–Sham equations to propagate the electron density in real time in the presence of the oscillating field of the laser pulse. The latter uses the time-dependent Schrödinger equation to propagate the wavefunction which is expanded in terms of the field-free electronic configurations of the molecule. Complex absorbing potentials (CAP)¹⁸ are used in both approaches to absorb the density or wavefunction once it is far enough from the molecule and thereby simulate ionization. For single ionization, the simplest TDCI approach requires configuration interaction with all single excitations (CIS) and needs to include enough diffuse configurations to model the dynamics of the electron as it is propagated toward the complex absorbing boundary. We have used TDCIS with a complex absorbing potential to study the angular dependence of single ionization for a variety of systems.^{4,5,9–17} Typical simulations involve propagating wavefunctions with thousands of singly excited configurations for tens of thousands of time steps.

Though accurate methods are available to simulate double ionization processes for two-electron systems,^{19–40} these methods cannot be readily extended to multi-electron systems. Direct simulation of double ionization with the TDCI approach requires propagating a wavefunction with at least single and double excited configurations (CISD), which is practical only for small systems. For more typical molecules, millions of singly and doubly excited configurations would need to be propagated for tens of thousands of time steps. Since this is usually not practical, alternative methods need to be explored.

Sequential double ionization can be modeled by two separate TDCI or rt-TDDFT simulations. One electron is removed from the HOMO, HOMO–1, etc., leading to one or more states of the cation and yielding the probability of generating each cation state as a function of the laser field direction. Additional simulations for each of the relevant cation states are then used to model the different channels for the second ionization. We have used this approach to model the angular dependence of double ionization in benzene and in methyl iodide.^{4,5} If the dynamics between close-lying or degenerate states of the cations is important, then these states should be treated together in one simulation, rather than in separate simulations. While the TDCIS-CAP approach is appropriate for the first step of a sequential double ionization, a more flexible representation may be desirable for simulating the second ionization step.

The CISD-ionization potential (CISD-IP) method described by Krylov and co-workers⁴¹ provides a means of representing a collection of cation states using a common set of orbitals and treating these cation states on an equal footing. The CISD-IP wavefunction consists of a small subset of the single and double excited configurations of the neutral molecule. The cation states are represented as ionizing excitations from the neutral ground state. These are augmented by a full set of singly excited configurations for each cation state (corresponding to double excitations from the neutral ground state) to allow for orbital relaxation. These excited configurations of the cations can be used in time-dependent CISD-IP with a complex absorbing potential (TDCISDIP-CAP) calculations to simulate the dynamics and ionization of the cations, analogous to the way that CIS provides the configurations needed for single ionization of the neutral molecule.

Experimental investigations of sequential double ionization of neon find that the second electron is preferentially ejected in a direction perpendicular to that of the first electron.^{42,43} The

measured angle-dependent ionization yields have been previously compared to model calculations for noble gas atoms.^{44–46} Experimental studies of double ionization of aligned acetylene have determined angle-dependent ionization rates and fragment branching ratios.^{47,48} Time-dependent density functional theory (TDDFT) calculations of the angle dependence of the first and second ionizations compared well with the experimental results.⁴⁸ As proof of concept, the present work uses the TDCIS-CAP and TDCISDIP-CAP methods to simulate the angular dependence for the second step of sequential double ionization of neon and acetylene, i.e., for the ionizing neon cation and acetylene cation. Section II summarizes simulations with the TDCI approach, describes the complex absorbing potential and additional basis functions used for modeling ionization, and outlines the calculation and analysis of the ionization rates. To model the first ionization of neon by linearly polarized light, we chose to remove an electron from the $2p_y^\beta$ orbital. To avoid any spurious dynamics due to non-stationary states, the TDCI simulation of the second ionization was started from the eigenstate of the cation that is dominated by the $2p_y^\beta$ hole. Ionization of the cation was found to occur primarily from a p orbital perpendicular to the p orbital involved in the first ionization, in agreement with the experimental observations. Similarly, for acetylene, the first electron was removed from the π_y^β orbital and the TDCI simulation of the second ionization was started from the eigenstate of the cation that is dominated by the π_y^β hole. In agreement with the experiment, ionization of the acetylene cation occurred primarily from the π orbital perpendicular to the π orbital involved in the first ionization.

II. METHODS

A. Time-dependent configuration interaction (TDCI)

In the TDCI-CAP approach, the time-dependent wavefunction is expanded on the basis of ground and excited configurations,

$$\Psi(t) = \sum_I C_I(t) |\Psi_I\rangle, \quad (1)$$

and is numerically integrated with the time-dependent Schrödinger equation,

$$\Psi(t) = \exp\left[-\frac{i}{\hbar} \int_{t_0}^t d\tau \left(\widehat{H}_{el} - \hat{\mu} \cdot \vec{E}(\tau) - i\widehat{V}^{abs}\right)\right] \Psi(t_0). \quad (2)$$

Here, \widehat{H}_{el} is the field-free molecular Hamiltonian for a fixed nuclear configuration. Molecular interaction with the field is described within the semiclassical dipole approximation $\hat{\mu} \cdot \vec{E}(\tau)$, where $\hat{\mu}$ is the dipole operator and $\vec{E}(\tau)$ is the time-dependent applied electric field. Ionization is captured with the complex absorbing potential (CAP), $i\widehat{V}^{abs}$, which absorbs the wavefunction as an electron is propagated away from the molecule. Using the modified-midpoint approximation, the wavefunction is incrementally propagated with a timestep of Δt ,

$$\Psi(t + \Delta t) = \exp\left[-\frac{i}{\hbar} \left(\widehat{H}_{el} - \hat{\mu} \cdot \vec{E}\left(t + \frac{\Delta t}{2}\right) - i\widehat{V}^{abs}\right)\right] \Psi(t), \quad (3)$$

and the exponential is approximated with Trotter–Suzuki factorization.⁴⁹ The final equation of motion can be expressed in matrix notation as

$$\begin{aligned} \mathbf{C}(t + \Delta t) = & \exp\left[-\frac{i\Delta t}{2\hbar}\mathbf{H}_{el}\right]\exp\left[-\frac{\Delta t}{2\hbar}\mathbf{V}^{abs}\right]\mathbf{W}^T\exp\left[-\frac{i}{\hbar}E\left(t + \frac{\Delta t}{2}\right)\mathbf{d}\right] \\ & \times \mathbf{W}\exp\left[-\frac{\Delta t}{2\hbar}\mathbf{V}^{abs}\right]\exp\left[-\frac{i\Delta t}{2\hbar}\mathbf{H}_{el}\right]\mathbf{C}(t), \end{aligned} \quad (4)$$

where $\mathbf{C}(t)$ is a column vector of CI coefficients and \mathbf{d} is a diagonal matrix of dipole eigenvalues obtained from $\mathbf{d} = \mathbf{W}\boldsymbol{\mu}\mathbf{W}^T$, where \mathbf{W} is the matrix of eigenvectors.

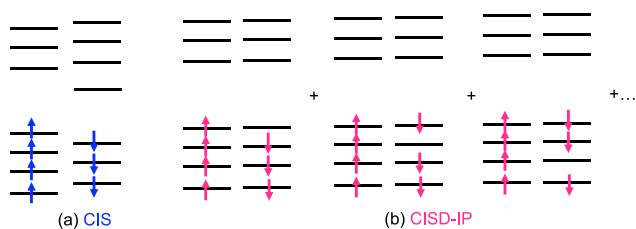
B. Complex absorbing potential and absorbing basis set

The absorbing potential is constructed from a set of overlapping potentials on each atom as described in previous studies.^{9–17} The value of the molecular absorbing potential is set to the minimum of values of the atomic absorbing potentials. The atomic potential for each atom is spherical and is zero for radial distances less than R_0 , where R_0 is set to be 3.5 times the atomic van der Waals radius. The potential beyond R_0 rises quadratically to 5 hartree at approximately $R_0 + 14.2$ bohrs. The potential turns over quadratically to a constant value of 10 hartree at approximately $R + 28.3$ bohrs. In this work, R_0 is taken to be 10.72 bohrs for neon, 12.735 bohrs for carbon, and 9.544 bohrs for hydrogen (i.e., 3.5 times the van der Waals radius).

For simulations with TDCI-CAP, additional diffuse basis functions are required in addition to the standard basis set in order for the system to interact with the complex absorbing potential. Appropriate absorbing basis sets were developed and tested in previous studies.^{10,14} For all simulations in this work, this absorbing basis set consists of four s functions with exponents of 0.0256, 0.0128, 0.0064, and 0.0032; four p functions with exponents of 0.0256, 0.0128, 0.0064, and 0.0032; four d functions with exponents of 0.0512, 0.0256, 0.0128, and 0.0064; and two f functions with exponents of 0.0256 and 0.0128. These basis functions were placed on each atom in addition to the standard aug-cc-pVTZ basis set.⁵⁰

C. CIS and CISD-IP Hamiltonians

The TDCI-CAP simulations for the second ionization are carried out using either the CIS or the CISD-IP states in Eq. (1). The TDCI-CAP method employs the molecular orbitals and energies of the Hartree–Fock (HF) ground state of the cation [Scheme 1(a)]. The wavefunction is expanded with the corresponding ground HF



SCHEME 1. (a) TDCI-CAP simulations for ionization of the cation include the UHF reference determinant for a specific cation state and all single excitations from this determinant. (b) TDCI-CAP simulations for ionization of the cation include the determinants obtained by removing one electron from β orbitals of the neutral molecule and all unique single excitations from these determinants.

and all singly excited determinants (CIS),

$$\Psi(t) = \sum_I C_I(t)|\Psi_I\rangle = c_0(t)|\Psi_0\rangle + \sum_{i,a} c_i^a(t)|\Psi_i^a\rangle. \quad (5)$$

The CIS Hamiltonian matrix elements are given by

$$\begin{aligned} \langle\Psi_0|\widehat{H}_{el}|\Psi_0\rangle &= E_0, & \langle\Psi_0|\widehat{H}_{el}|\Psi_j^b\rangle &= 0, \\ \langle\Psi_i^a|\widehat{H}_{el}|\Psi_j^b\rangle &= (E_0 - \epsilon_i + \epsilon_a)\delta_{ij}\delta_{ab} - \langle ja||ib\rangle, \end{aligned} \quad (6)$$

where E_0 is the ground state energy of the cation, ϵ are orbital energies, $\{i,j\}$ refer to occupied molecular orbitals, and $\{a,b\}$ refer to virtual molecular orbitals. The double bar integrals are

$$\langle rs||tu\rangle = \int dr_1 dr_2 \phi_r^*(r_1)\phi_s^*(r_2) \frac{1}{r_{12}} [\phi_t(r_1)\phi_u(r_2) - \phi_u(r_1)\phi_t(r_2)]. \quad (7)$$

The one-electron matrix elements for the absorbing potential and the dipole are given by

$$\begin{aligned} \langle\Psi_0|\widehat{A}|\Psi_0\rangle &= A_{00} = \sum_i^{occ} \langle i|\widehat{A}|i\rangle, \\ \langle\Psi_0|\widehat{A}|\Psi_i^a\rangle &= \langle i|\widehat{A}|a\rangle, \\ \langle\Psi_i^a|\widehat{A}|\Psi_j^b\rangle &= A_{00}\delta_{ij}\delta_{ab} - \langle j|\widehat{A}|i\rangle\delta_{ab} + \langle a|\widehat{A}|b\rangle\delta_{ij}, \end{aligned} \quad (8)$$

where the one-electron integrals are $\langle r|\widehat{A}|s\rangle = \langle\phi_r|\widehat{A}|\phi_s\rangle = \int dr_1 \phi_r^*(r_1)\widehat{A}\phi_s(r_1)$.

The CISD-IP Hamiltonian, as described by Krylov and co-workers,⁴¹ is constructed from the molecular orbitals and energies computed from the Hartree–Fock (HF) ground state of the neutral molecule, and includes all unique 1-hole, 2-hole, 1-particle determinants [Scheme 1(b)],

$$\Psi(t) = \sum_I C_I(t)|\Psi_I\rangle = \sum_x c_x(t)|\Psi_x\rangle + \sum_{i<x,a} c_{ix}^a(t)|\Psi_{ix}^a\rangle, \quad (9)$$

where the 1-hole determinants represent ionized configurations and 2-hole and 1-particle determinants represent singly excited ionized configurations. With these states, the matrix elements of the molecular Hamiltonian can be expressed as

$$\begin{aligned} \langle\Psi_x|\widehat{H}_{el}|\Psi_y\rangle &= (E_0 - \epsilon_x)\delta_{xy}, \\ \langle\Psi_x|\widehat{H}_{el}|\Psi_{jy}^b\rangle &= \langle jy||xb\rangle, \\ \langle\Psi_{ix}^a|\widehat{H}_{el}|\Psi_{jy}^b\rangle &= (E_0 - \epsilon_i - \epsilon_x + \epsilon_a)\delta_{ij}\delta_{xy}\delta_{ab} + \langle jy||xi\rangle\delta_{ab} \\ &\quad - \langle ja||ib\rangle\delta_{xy} - \langle ya||xb\rangle\delta_{ij} + \langle ja||xb\rangle\delta_{iy} + \langle ya||ib\rangle\delta_{xj}, \end{aligned} \quad (10)$$

where E_0 is the HF energy of the neutral ground state, $\{x,y\}$ refers to ionized (hole) beta molecular orbitals, and $i < x$ and $j < y$ for the beta orbitals. The one-electron matrix elements are given by

$$\begin{aligned} \langle\Psi_x|\widehat{A}|\Psi_y\rangle &= A_{00}\delta_{xy} - \langle y|\widehat{A}|x\rangle, \\ \langle\Psi_x|\widehat{A}|\Psi_{jy}^b\rangle &= \langle j|\widehat{A}|b\rangle\delta_{xy} - \langle y|\widehat{A}|b\rangle\delta_{jx}, \\ \langle\Psi_{ix}^a|\widehat{A}|\Psi_{jy}^b\rangle &= A_{00}(\delta_{ij}\delta_{xy}\delta_{ab}) - \langle j|\widehat{A}|i\rangle\delta_{xy}\delta_{ab} + \langle a|\widehat{A}|b\rangle\delta_{ij}\delta_{xy} \\ &\quad - \langle y|\widehat{A}|x\rangle\delta_{ij}\delta_{ab} + \langle y|\widehat{A}|i\rangle\delta_{jx}\delta_{ab} + \langle j|\widehat{A}|x\rangle\delta_{iy}\delta_{ab}. \end{aligned} \quad (11)$$

D. Ionization rates

In this work, the instantaneous ionization rate is defined as the change in the norm squared of the wavefunction,

$$\text{rate} = \frac{d}{dt} N(t)^2 = -\frac{2}{\hbar} \langle \Psi(t) | \widehat{V}^{abs} | \Psi(t) \rangle / \langle \Psi(t) | \Psi(t) \rangle. \quad (12)$$

The total ionization rate for a normalized CIS wavefunction in terms of the one-electron integral of the absorbing potential is

$$\begin{aligned} \left\langle \frac{d}{dt} N(t)^2 \right\rangle = & -\frac{2}{\hbar} \left[c_0^*(t) c_0(t) V_{00}^{abs} + \sum_{ia} (c_i^{a*}(t) c_0(t) + c_0^*(t) c_i^a(t)) \right. \\ & \times \langle i | \widehat{V}^{abs} | a \rangle + \sum_{ijab} c_i^{a*}(t) c_j^b(t) \\ & \left. \times (V_{00}^{abs} \delta_{ij} \delta_{ab} - \langle j | \widehat{V}^{abs} | i \rangle \delta_{ab} + \langle a | \widehat{V}^{abs} | b \rangle \delta_{ij}) \right], \quad (13) \end{aligned}$$

where $V_{00}^{abs} = \sum_i^{occ} \langle i | \widehat{V}^{abs} | i \rangle$. The total rate can be partitioned into contributions to ionization from each of the occupied orbitals,

$$\begin{aligned} \left\langle \frac{d}{dt} N(t)^2 \right\rangle_i = & -\frac{2}{\hbar} \left[\langle i | \widehat{V}^{abs} | i \rangle + \sum_a 2 \Re e (c_i^{a*}(t) c_0(t)) \langle i | \widehat{V}^{abs} | a \rangle \right. \\ & - \sum_{ja} \Re e (c_i^{a*}(t) c_j^a(t)) \langle i | \widehat{V}^{abs} | j \rangle \\ & \left. + \sum_{ab} \Re e (c_i^{a*}(t) c_i^b(t)) \langle a | \widehat{V}^{abs} | b \rangle \right]. \quad (14) \end{aligned}$$

This can be interpreted as the rate of formation of an ionized state with a hole in orbital i .

For a normalized CISD-IP wavefunction, the total ionization rate is

$$\begin{aligned} \left\langle \frac{d}{dt} N(t)^2 \right\rangle = & -\frac{2}{\hbar} \left[\sum_{x,y} c_x^*(t) c_y(t) \langle \psi_x | \widehat{V}^{abs} | \psi_y \rangle \right. \\ & + \sum_{i<x,y,a} c_{ix}^{a*}(t) c_y(t) \langle \psi_{ix}^a | \widehat{V}^{abs} | \psi_y \rangle \\ & + \sum_{x_j<y,b} c_x^*(t) c_{jy}^b(t) \langle \psi_x | \widehat{V}^{abs} | \psi_{jy}^b \rangle \\ & \left. + \sum_{i<x_j<y,a,b} c_{ix}^{a*}(t) c_{jy}^b(t) \langle \psi_{ix}^a | \widehat{V}^{abs} | \psi_{jy}^b \rangle \right]. \quad (15) \end{aligned}$$

This can be partitioned into the rate of formation of dication species with holes in orbitals x and i ,

$$\begin{aligned} \left\langle \frac{d}{dt} N(t)^2 \right\rangle_{x,i} = & -\frac{2}{\hbar} \left[c_x^*(t) c_x(t) \langle i | \widehat{V}^{abs} | i \rangle + c_i^*(t) c_i(t) \langle x | \widehat{V}^{abs} | x \rangle \right. \\ & - \Re e (c_x^*(t) c_i(t) + c_i^*(t) c_x(t)) \langle i | \widehat{V}^{abs} | x \rangle \\ & + \sum_{y,a} 2 \Re e (c_{ix}^{a*}(t) c_y(t)) \langle \psi_{ix}^a | \widehat{V}^{abs} | \psi_y \rangle \\ & \left. + \sum_{j<y,a,b} \Re e (c_{ix}^{a*}(t) c_{jy}^b(t)) \langle \psi_{ix}^a | \widehat{V}^{abs} | \psi_{jy}^b \rangle \right]. \quad (16) \end{aligned}$$

For field-free simulations, there is a small residual rate arising from the interaction of the ground state with the absorbing potential. This

residual rate is subtracted from the rate in the field to obtain the net mean ionization rate,

$$\left\langle \frac{d}{dt} N(t)^2 \right\rangle = \left\langle \frac{d}{dt} N(t)^2 \right\rangle_{\text{field}} - \left\langle \frac{d}{dt} N(t)^2 \right\rangle_{\text{field-free}}. \quad (17)$$

E. Computational details

Molecular orbitals and energies, one and two-electron integrals, and absorbing potential integrals were calculated with a locally modified copy of the Gaussian program suite.⁵¹ Closed shell systems were calculated with spin-restricted methods and open shell systems were calculated with spin-unrestricted methods. A stand-alone Fortran 95 code used in our previous TDCIS-CAP studies^{4,5,9-17} was extended to include the CISD-IP Hamiltonian.⁴¹ This code was used to integrate the TDCI equations and analyze the TDCI results. The wavefunction was propagated in the oscillating electric field of a laser pulse for 16 000 steps using a time step of $t = 0.05$ a.u. (1.2 as), for a total simulation time of 19.35 fs (800 a.u.). The test in prior studies showed that reducing the time step by half changed the norm at the end of the simulation by less than 0.01%.^{14,16} A 800 nm laser pulse was modeled by a linearly polarized oscillating electric field with a trapezoidal pulse,

$$E(t) = \begin{cases} \left(\frac{t}{\tau_p}\right) E_{\max} \cos(\omega t), & 0 \leq t \leq \tau_p \\ E_{\max} \cos(\omega t), & \tau_p < t \leq 6\tau_p \\ \left(7 - \frac{t}{\tau_p}\right) E_{\max} \cos(\omega t), & 6\tau_p < t \leq 7\tau_p \\ 0, & 7\tau_p < t \end{cases} \quad (18)$$

with a period of $\tau_p = 2\pi/\omega$ and maximum field strength of E_{\max} was applied for 7 cycles for all systems. In this work, the mean ionization rates used in Eq. (17) correspond to the average of the instantaneous rates computed every 50 timesteps (60 as) for the duration of the sixth cycle of the field. For neon, the mean ionization rates in the z direction are 0.06975 fs^{-1} for TDCIS-CAP at $E_{\max} = 0.40$ a.u. and 0.07078 fs^{-1} for TDCISDIP-CAP at $E_{\max} = 0.50$ a.u. The norms squared after the pulse are 0.4133 and 0.4078, respectively; the residual field-free rates are 0.001699 fs^{-1} and 0.001215 fs^{-1} , respectively. For C_2H_2 , the mean ionization rates in the x direction are 0.09392 fs^{-1} for TDCIS-CAP at $E_{\max} = 0.105$ a.u. and 0.04554 fs^{-1} for TDCISDIP-CAP at $E_{\max} = 0.115$ a.u. The norms squared after the pulse are 0.3279 and 0.5748, respectively; the residual field-free rates are $0.0007968 \text{ fs}^{-1}$ and $0.00096511 \text{ fs}^{-1}$, respectively.

III. RESULTS AND DISCUSSION

A. Ionization of the neon cation, Ne^+

The electron dynamics of the ionization of the neon cation by a strong laser field were simulated with the TDCIS-CAP and TDCISDIP-CAP approaches. For the TDCIS-CAP simulation, the matrix elements of the Hamiltonian and the field-free singly excited states were computed from the molecular orbitals, energies, and integrals from a spin-unrestricted Hartree-Fock calculation of the cation with the hole localized in the $2p_y^\beta$ orbital. For the TDCISDIP-CAP simulation, the Hamiltonian and field-free excited states were computed from a spin-restricted Hartree-Fock calculation of the

closed shell neutral atom. The lowest three states of the CISD-IP Hamiltonian are degenerate and are dominated by a hole in the $2p_x$, $2p_y$, and $2p_z$ orbitals. The initial wavefunction for the TDCISDIP-CAP was set to be $|\Psi(0)\rangle \approx 0.971|\Psi_{2p_y^\beta}\rangle$. In total, 869 CIS states and 3365 CISD-IP states were included in the simulations.

In Table I, the first ionization potentials (IP) calculated by Δ CCSD(T), the difference in the coupled cluster singles and doubles with perturbative triples [CISD(T)] energies of neon neutral and the neon cation are in very good agreement with the experimental values.⁵² The IP calculated by Δ SCF is lower than the IP calculated by the Koopmans theorem due to orbital relaxation in the SCF calculation of the cation. Since the TDCIS simulation starts with a Hartree-Fock calculation of the cation, the first IP listed for CIS is the same as the Δ SCF value. The IP calculated by CISD-IP is lower than the Δ SCF value because it includes some electron correlation for the cation. For second ionization potentials, there are three states to consider for the neon dication. Removing two electrons from the $2p^\beta$ orbitals of the neutral atom yields a component of the 3P state. Components of the 1D and 1S states can be obtained by removing an α electron and a β electron from the set of $2p$ orbitals. Spin-unrestricted SCF and CCSD(T) calculations of the triplet dication yield estimates for the IP from the cation to the 3P dication, while singlet spin-restricted SCF and CCSD(T) calculations of the dication yield IP estimates for the 1D state but not the 1S state. Koopmans theorem applied to the cation provides estimates for the second IP. Similar to the first IP, Δ CCSD(T) calculations for the second IP are in very good agreement with the experimental values for the 3P and 1D dications.^{53,54}

Estimates of the second IP for the CIS and CISD-IP calculations can be obtained with the help of the absorbing potential matrix elements. The large absorbing basis set yields series of singly excited states that interact more strongly with the absorbing potential as they approach the ionization limit. Figure 1 shows the energies of the CIS and CISD-IP states and their absorbing potential matrix elements, $\langle V^{abs} \rangle$, as a function of the state number. The ionization potential for a particular series is obtained from the state energy where the absorbing potential reaches a maximum. The three series in Fig. 1 correspond to ionization of the cation to the 3P , 1D , and 1S dications. For CIS, the second IPs are about 1.5 eV lower than

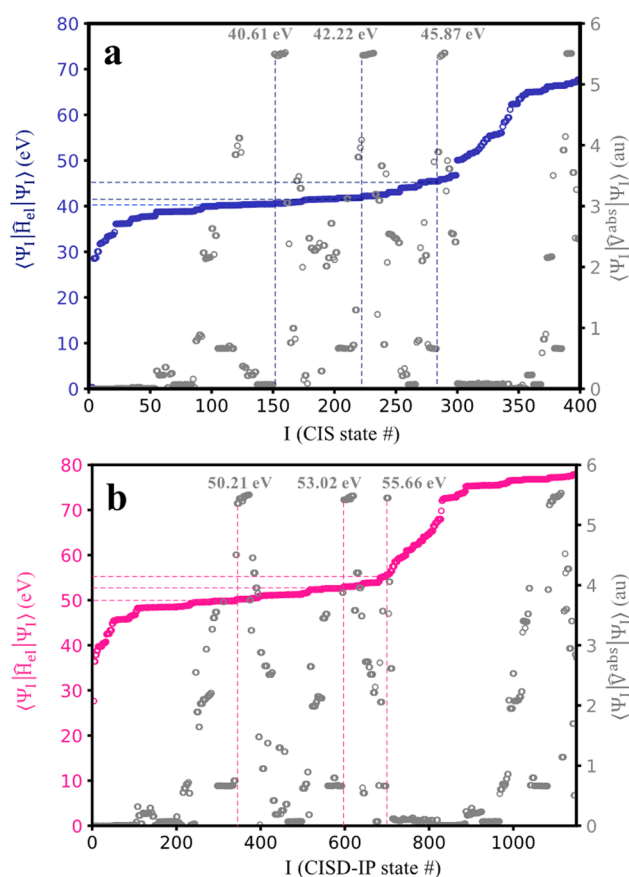


FIG. 1. Expectation value of the absorbing potential computed for the (a) CIS and (b) CISD-IP states with respect to the CIS (blue) and CISD-IP (pink) field-free state energies. Both sets of energies are shown with respect to the first ionization potentials of 19.69 eV and 18.57 eV for CIS and CISD-IP, respectively.

TABLE I. First and second ionization potentials of neon (in eV).

Method	First ionization potential (eV)	Second ionization potential (eV) with respect to first IP		
		3P	1D	1S
Δ SCF ^a	19.69	39.27	44.57	...
Koopmans ^a	23.16	42.10	43.72	47.38
CIS	19.69	~40.61	~42.22	~45.87
CISD-IP	18.57	~50.21	~53.02	~55.66
Δ CCSD(T) ^a	21.46	40.73	44.11	...
Experimental ^b	21.56	40.96	44.17	47.87

^aCalculated with the aug-cc-pVTZ basis.

^bReferences 52–54.

the Koopmans theory values, indicating that the diffused states are strongly absorbed a little before they reach the ionization limit. The second IPs for CISD-IP are about 10 eV higher than the CIS values for a combination of reasons. The CIS wavefunction uses the relaxed orbitals from the SCF calculation of the cation, whereas the CISD-IP wavefunction uses the unrelaxed orbitals from the neutral atom. In addition, the CISD-IP includes some electron correlation for the cation but not the dication. Since the second IPs are too high with CISD-IP, the calculated ionization rates will be too low. Therefore, we restrict the discussion to relative rates and the angular dependence of the ionization.

Figures 2(a) and 3(a) show the angular dependence of the second ionization of the $2p_y^\beta$ neon cation in the yz plane (yx plane is equivalent by symmetry). The field strengths vary from 0.1 a.u. to 0.4 a.u. for TDCIS-CAP and 0.1 a.u. to 0.5 a.u. for TDCISDIP-CAP. For a given field strength, TDCISD-IP ionization rates are much smaller than those of TDCIS-CAP because of the difference in the second ionization potential calculated by these methods. However, the angular dependence of the ionization rate is similar, with a

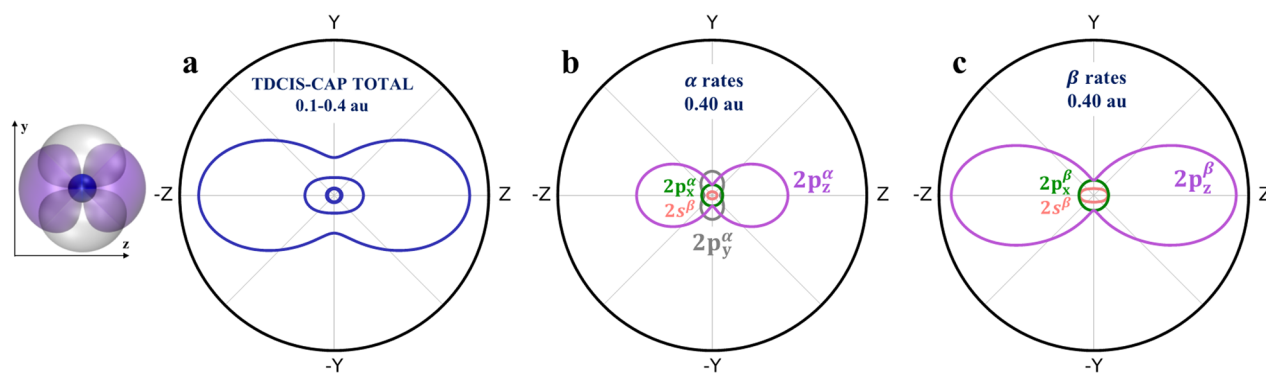


FIG. 2. TDCIS-CAP (a) angular dependence of ionization of $2p_y^\beta \text{Ne}^+$ for four field strengths of (from inner to outer) 0.10 a.u., 0.20 a.u., 0.30 a.u., and 0.40 a.u. (b) Angular dependence of second ionization from the alpha molecular orbitals for a field strength of 0.40 a.u. (c) Angular dependence of second ionization from the beta molecular orbitals for a field strength of 0.40 a.u.

maximum when the field is polarized in the z direction and a minimum when the field is polarized in the y direction. This compares well with the angular dependence of the ionization rate extrapolated from the experimental data.⁴²

The total ionization rate can be decomposed into contributions from the α and β orbitals using Eqs. (14) and (16) as shown in Figs. 2(b) and 2(c) for TDCIS-CAP and Figs. 3(b) and 3(c) for TDCISDIP-CAP. The initial state of the neon cation has an empty $2p_y^\beta$ orbital. For both TDCIS-CAP and TDCISDIP-CAP, the largest contribution in the yz plane is ionization from the $2p_z^\beta$ orbital yielding a component of the ^3P dication state [Figs. 2(c) and 3(c)]. The next largest contribution in the yz plane is from ionization of the $2p_x^\alpha$ orbital yielding a component of the ^1D dication state [Figs. 2(b) and 3(b)]. Corresponding contributions to the ^3P and ^1D cations come from the $2p_x^\beta$ and $2p_x^\alpha$ orbitals in the xy plane. Ionization from the $2p_y^\alpha$ orbital yields the ^1S dication. This component is larger in the TDCISDIP-CAP simulation and partially accounts for the smaller

difference in second ionization rates between the y direction and z direction when compared to TDCIS-CAP.

Because of the larger number of configurations, the TDCISDIP-CAP simulation has some features that are lacking in the TDCIS-CAP simulation. Figure 4 shows the population of the $2s^\beta$, $2p_x^\beta$, $2p_y^\beta$, and $2p_z^\beta$ orbitals as a function of the field direction for five different times. Initially, the population of the $2p_y^\beta$ orbital is near zero and the populations of the $2s^\beta$, $2p_x^\beta$, and $2p_z^\beta$ orbitals are near one. The population of the $2s^\beta$ and $2p_x^\beta$ orbitals remains constant and independent of the angle of the field in the yz plane. For the field in the y or z directions, the population of the $2p_y^\beta$ orbital stays small and the population of the $2p_z^\beta$ orbital stays near one. However, for intermediate angles, the population of the $2p_z^\beta$ orbital decreases with time and the population of the $2p_y^\beta$ orbital increases. This corresponds to a rotation between degenerate states of the neon cation (i.e., change in the direction of the $2p^\beta$ hole) in response to the angle of the laser field.

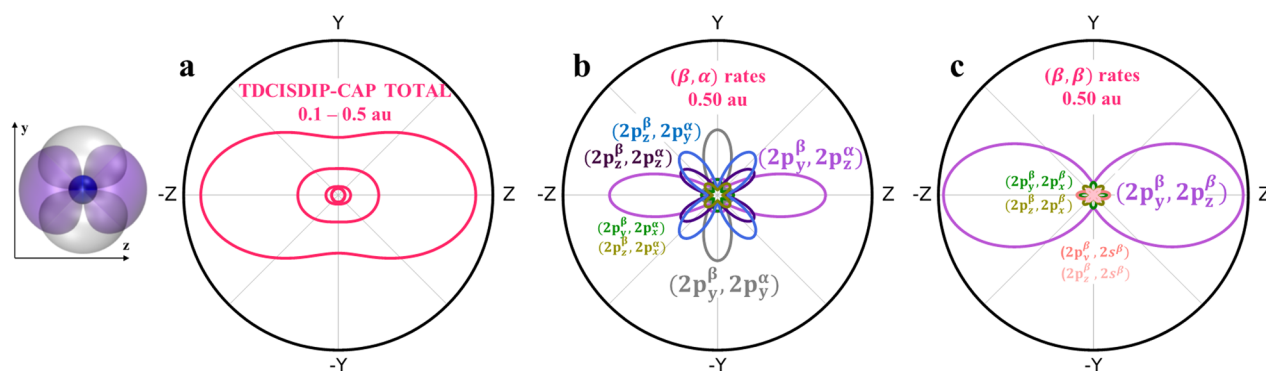


FIG. 3. TDCISDIP-CAP (a) angular dependence of ionization of $2p_y^\beta \text{Ne}^+$ for five field strengths of (from inner to outer) 0.10 a.u., 0.20 a.u., 0.30 a.u., 0.40 a.u., and 0.50 a.u. (b) Angular dependence of second ionization to form dication species with holes in α and β orbitals for a field strength of 0.50 a.u. (c) Angular dependence of second ionization to form dication species with holes in β orbitals for a field strength of 0.50 a.u.

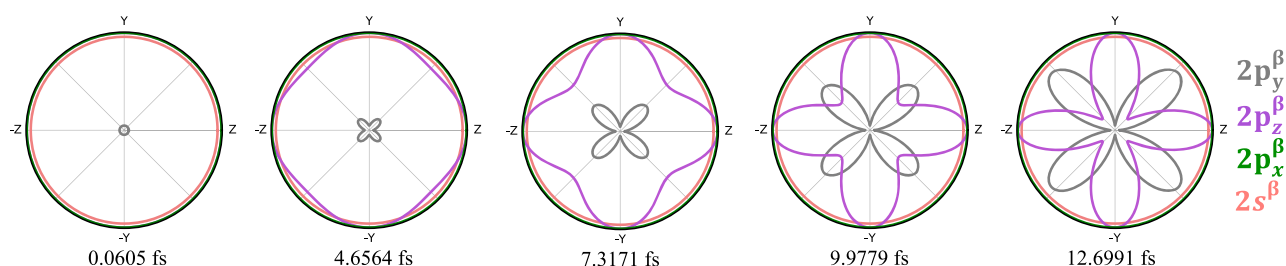


FIG. 4. Population of β molecular orbitals with respect to time. The angles of the polar plot correspond to the polarization direction of the field. The radial distance corresponds to the orbital population and increases from 0 (unoccupied) to 1 (fully occupied). The field is close to zero for the selected times.

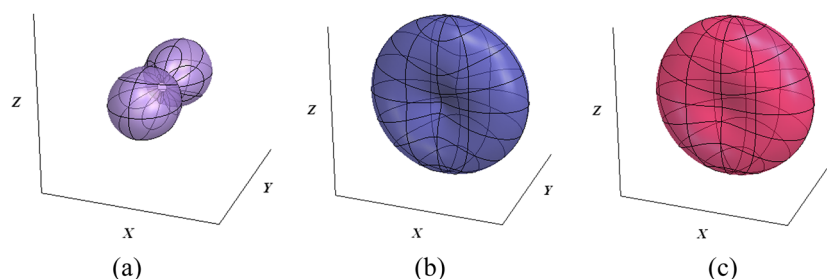


FIG. 5. Angular dependence of ionization yield for neon (a) TDCIS-CAP calculation of the first ionization (contribution arising from removing an electron from the $2p_y^\beta$ orbital), (b) TDCIS-CAP and (c) TDCISD-IP calculations of the second ionization (contribution arising from removing an electron from the $2p_y^\beta$ cation of neon). To facilitate the comparison of the shapes, the ionization yields have been scaled so that the maximum values are equal.

The polarizability is less in the direction of the $2p^\beta$ hole and greater in the direction perpendicular to it. The rotational force on the electron density or on the direction of the $2p^\beta$ hole resulting from the laser field is maximal at 45° to the axis of the $2p^\beta$ hole, similar to the rotational force on a homonuclear diatomic molecule in an electric field. CISDIP treats the interaction of the degenerate cation states with the field on an equal footing, but CIS treats only one of the degenerate states of the cation with the same accuracy as CISDIP.

Three dimensional views of the ionization yield are shown in Fig. 5. For a TDCIS-CAP simulation of the first ionization of an electron from the $2p_y^\beta$ orbital of neutral neon, the angular dependence resembles the $2p_y^\beta$ orbital as expected. In simulations of the second ionization of neon, the electron is ionized predominantly from orbitals perpendicular to the one involved in the first ionization, in this case the $2p_x^\beta$ and $2p_z^\beta$ orbitals. The TDCISDIP-CAP shows a bit more ionization in the y direction resulting from greater contributions from the α orbitals, as can be seen by comparing Figs. 2(b) and 3(b).

B. Ionization of the acetylene cation, $C_2H_2^+$

The ionization potentials for acetylene are listed in Table II. The lowest energy states of the cation and dication involve ionization of electrons from the π orbitals. The first IPs calculated by Δ CCSD(T) and Koopmans theorem are in very good agreement with the experimental value,⁵² while the Δ SCF and CISD-IP estimates are too low. The π^2 dication of acetylene is isoelectronic with O_2 and has $^3\Sigma$, $^1\Delta$, and $^1\Sigma$ as the three lowest states. Removing one electron from

the π_x^β orbital and one electron from the π_y^β orbital of the neutral acetylene yields a component of the $^3\Sigma$ state. Components of the $^1\Delta$ and $^1\Sigma$ states can be obtained by removing one electron from a π^α orbital and one electron from a π^β orbital. The Δ CCSD(T) and Koopmans theory values for the second IP are in good agreement with the experimental value.^{55–57} Similar to neon, the estimates of the second IP for CIS and CISD-IP calculations can be obtained by comparing the energies and the absorbing potential matrix elements, as shown in Fig. 6. The second IPs are about 1.5–2 eV too low for CIS and about 2 eV too high for CISD-IP.

TABLE II. First and second ionization potentials of acetylene (in eV).

Method	First ionization potential (eV)	Second ionization potential (eV) with respect to first IP		
		$^3\Sigma$	$^1\Delta$	$^1\Sigma$
Δ SCF ^a	9.77	19.22	21.14	...
Koopmans ^a	11.17	20.45	20.98	22.35
CIS	9.77	~19.15	~19.65	~21.02
CISD-IP	9.17	~23.26	~24.16	~25.05
Δ CCSD(T) ^a	11.44	20.96	22.10	...
Experimental ^b	11.4	20.3, 21.3	22.0	

^aCalculated with the aug-cc-pVTZ basis.

^bReferences 52 and 55–57.

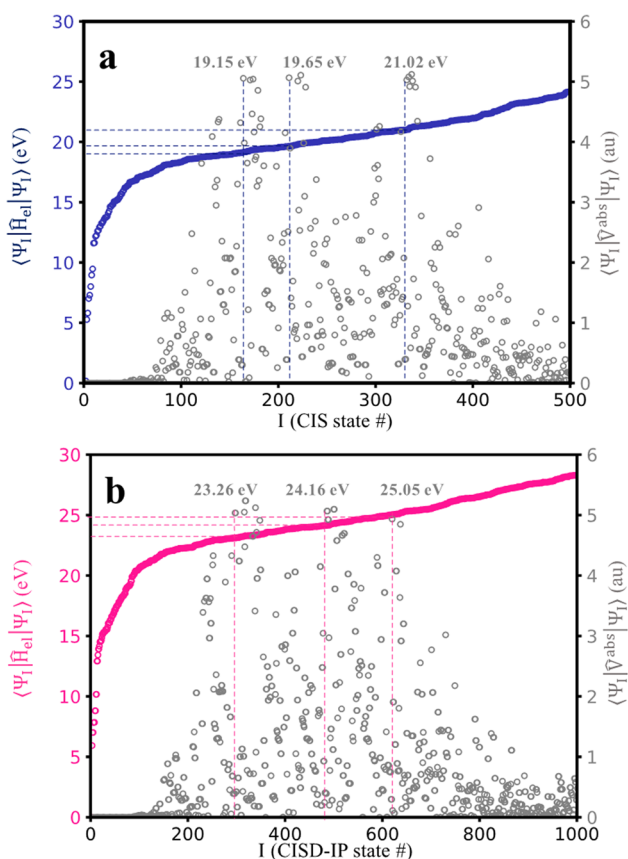


FIG. 6. Expectation value of the absorbing potential computed for the (a) CIS and (b) CISD-IP states with respect to the CIS (blue) and CISD-IP (pink) field-free state energies. Both sets of energies are shown with respect to the first ionization potentials of 9.764 eV and 9.165 eV for CIS and CISD-IP, respectively.

The initial wavefunction for TDCIS-CAP started with the hole localized in the π_y^β orbital and TDCISDIP-CAP started from the state $|\Psi(0)\rangle \approx 0.969|\Psi_{\pi_y^\beta}\rangle$. The molecular axis of acetylene is placed along the z axis and the angular dependence of second ionization obtained

from TDCIS-CAP and TDCISDIP-CAP simulations are shown in Figs. 7(a) and 8(a), respectively, for the xy plane. The TDCIS-CAP simulation used 2426 configurations and 7 field strengths varying uniformly from 0.085 a.u. to 0.115 a.u.; TDCSDIP-CAP simulations used 9420 configurations and the field strength from 0.095 a.u. to 0.125 a.u. Similar to the neon cation, the computed TDCIS-CAP ionization rates for the acetylene cation are larger than those of TDCISDIP-CAP due to the differences in the second IPs. The initial state of the acetylene cation was chosen to have an empty π_y^β orbital. For both the TDCIS-CAP and TDCISDIP-CAP simulations for ionization of the acetylene cation, the largest contribution in the xy plane is the removal of an electron from the π_x^β orbital yielding a component of the $^3\Sigma$ state [Figs. 7(c) and 8(c)]. The next largest contribution in the xy plane is from ionization of the π_x^α orbital yielding a component of the $^1\Delta$ dication state [Figs. 7(b) and 8(b)]. Removing an electron from the π_y^α yields a component of the $^1\Sigma$ dication.

Similar to the neon cation, the TDCISDIP-CAP simulation of ionization of the acetylene cation shows some evidence of rotation of the π^β hole. Figure 9 shows the population of the π_x^β and π_y^β orbitals as a function of the field direction for five different times. Initially the population of the π_x^β and π_y^β orbitals are approximately 1 and 0, respectively. For the field in the x or y direction, the populations of these orbitals change very little. For intermediate angles, the population of the π_x^β orbital decreases with time and the population of the π_y^β orbital increases, corresponding to a rotation of the π^β hole. However, the response is much smaller than that seen in the ionization of the neon cation (Fig. 4).

The angular dependence of the ionization yields for acetylene is shown in Fig. 10. The shape of the ionization yield for removing an electron from the π_y^β orbital resembles the shape of that orbital as expected. In the next ionization of this cation, the electron is removed predominantly from the π_x^β orbital which is perpendicular to the orbital involved in the first ionization. The TDCISDIP-CAP ionization yield is a little larger in the y direction, while the TDCIS-CAP ionization yield is a little larger in directions intermediate between x and z . Both show comparatively little ionization in the z direction, i.e., along the molecular axis, in keeping with the fact that the σ orbitals are significantly lower in energy than the π orbitals.

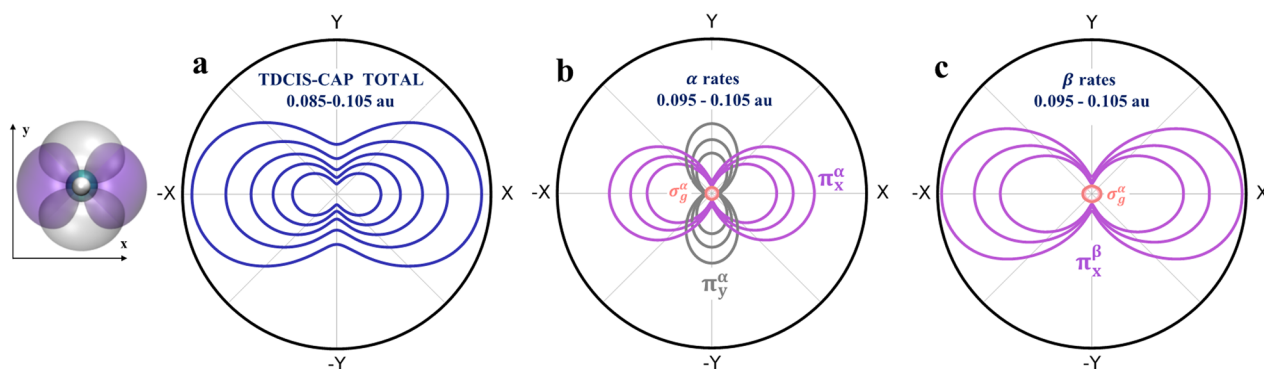


FIG. 7. TDCIS-CAP (a) angular dependence of second ionization of the $\pi_y^\beta\text{C}_2\text{H}_2$ cation for seven field strengths of (from inner to outer) 0.085 a.u., 0.090 a.u., 0.095 a.u., 0.100 a.u., 0.105 a.u., 0.110 a.u., and 0.115 a.u. (b) Angular dependence of second ionization from the alpha molecular orbitals for field strengths of (from inner to outer) 0.095 a.u., 0.100 a.u., and 0.105 a.u. (c) Angular dependence of second ionization from the beta molecular orbitals for field strengths of 0.095 a.u., 0.100 a.u., and 0.105 a.u.

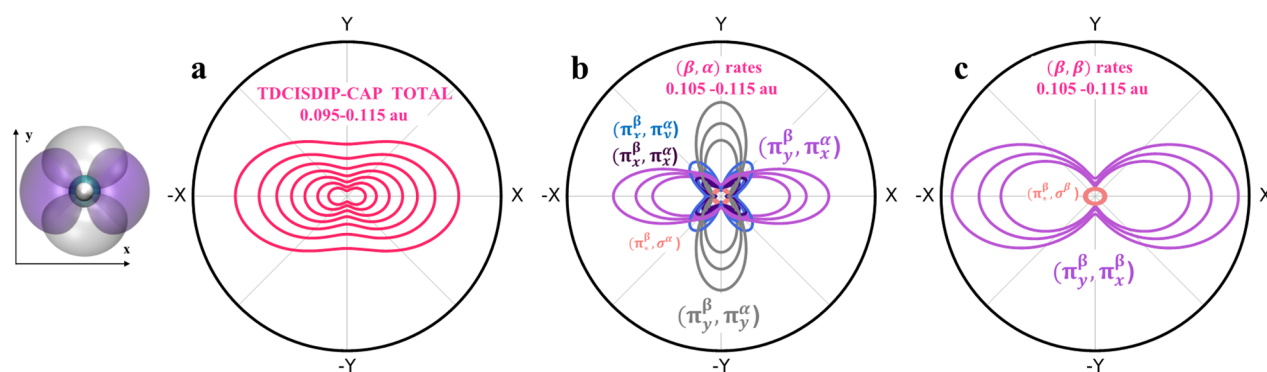


FIG. 8. TDCISDIP-CAP (a) angular dependence of second ionization of the $2\pi_y^{\beta}C_2H_2$ cation for seven field strengths of (from inner to outer) 0.095 a.u., 0.100 a.u., 0.105 a.u., 0.110 a.u., 0.115 a.u., 0.120 a.u., and 0.125 a.u. (b) Angular dependence of second ionization to form dication species with holes in the α and β orbitals for the field strengths of 0.105 a.u., 0.110 a.u., and 0.115 a.u. (c) Angular dependence of second ionization to form dication species with holes in the β orbitals for the field strengths of 0.105 a.u., 0.110 a.u., and 0.115 a.u.

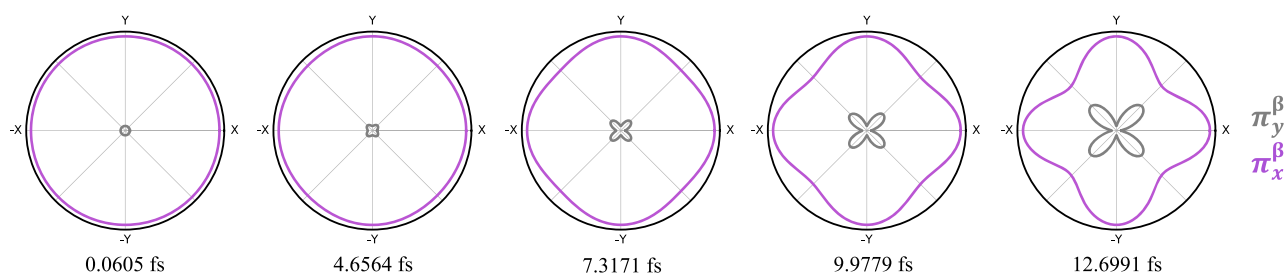


FIG. 9. Population of the π_x^{β} and π_y^{β} orbitals with respect to time. The angles of the polar plot correspond to the polarization direction of the field. The radial distances correspond to the orbital population and increases from 0 (unoccupied) to 1 (fully occupied). The field is close to zero for the selected times.

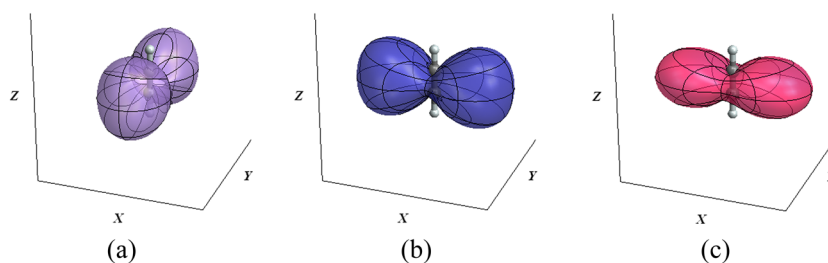


FIG. 10. Angular dependence of ionization yield for acetylene (a) TDCIS-CAP calculation of the first ionization (contribution arising from removing an electron from the π_y^{β} orbital), (b) TDCIS-CAP, and (c) TDCISD-IP calculations of the second ionization (contribution arising from removing an electron from the π_y^{β} cation of acetylene). To facilitate the comparison of the shapes, the ionization yields have been scaled so that the maximum values are equal.

IV. SUMMARY

This study has demonstrated the use of TDCIS-CAP and TDCISDIP-CAP to simulate the second ionization of neon and acetylene. The estimated CIS second ionization potential is generally lower than CISD-IP because the CIS calculation starts with the relaxed orbitals of the cation, whereas the CISD-IP calculation starts with the orbitals of the neutral molecule. Since the second

ionization potentials are larger for CISD-IP, higher intensities are needed to obtain second ionization rates comparable to the TDCIS-CAP simulations. Nevertheless, the two approaches yield similar angular dependence for the second ionization and show the second electron ionizing from the orbital perpendicular to the orbital involved in the first ionization. The TDCISDIP-CAP simulations of the angular dependence of the second ionization of neon and acetylene have some features arising from population (hole)

dynamics not present in the TDCIS-CAP simulations. Because the TDCISDIP-CAP simulations include all single excitations from each of the degenerate monocation states, the field can induce a rotation between degenerate states of the cation. By contrast, the TDCIS-CAP simulations include single excitations from only one of the degenerate cation states and cannot model this effect. This new method puts us one step closer to modeling fully correlated strong field double ionization processes. In future work, we plan to link the simulations for the first and second ionizations so that the CI vector for the ionized state from a TDCIS simulation of the first ionization will be used as input for the TDCISDIP simulation for the second ionization.

ACKNOWLEDGMENTS

This work was supported by a grant from the National Science Foundation (Grant No. CHE1856437). We thank the Wayne State University Computing Grid for access to high performance computing.

REFERENCES

- 1 T. Weber *et al.*, "Correlated electron emission in multiphoton double ionization," *Nature* **405**, 658 (2000).
- 2 W. Becker, X. Liu, P. J. Ho, and J. H. Eberly, "Theories of photoelectron correlation in laser-driven multiple atomic ionization," *Rev. Mod. Phys.* **84**, 1011 (2012).
- 3 Q. Liao, A. H. Winney, S. K. Lee, Y. F. Lin, P. Adhikari, and W. Li, "Coulomb-repulsion-assisted double ionization from doubly excited states of argon," *Phys. Rev. A* **96**, 023401 (2017).
- 4 A. H. Winney, S. K. Lee, Y. F. Lin, Q. Liao, P. Adhikari, G. Basnayake, H. B. Schlegel, and W. Li, "Attosecond electron correlation dynamics in double ionization of benzene probed with two-electron angular streaking," *Phys. Rev. Lett.* **119**, 123201 (2017).
- 5 A. H. Winney, G. Basnayake, D. A. Debrah, Y. F. Lin, S. K. Lee, P. Hoerner, Q. Liao, H. B. Schlegel, and W. Li, "Disentangling strong-field multielectron dynamics with angular streaking," *J. Phys. Chem. Lett.* **9**, 2539 (2018).
- 6 A. Sissay, P. Abanador, F. Mauger, M. Gaarde, K. J. Schafer, and K. Lopata, "Angle-dependent strong-field molecular ionization rates with tuned range-separated time-dependent density functional theory," *J. Chem. Phys.* **145**, 094105 (2016).
- 7 P. Sandor *et al.*, "Angle dependence of strong-field single and double ionization of carbonyl sulfide," *Phys. Rev. A* **98**, 043425 (2018).
- 8 P. Sandor *et al.*, "Angle-dependent strong-field ionization of halomethanes," *J. Chem. Phys.* **151**, 194308 (2019).
- 9 P. Krause and H. B. Schlegel, "Strong-field ionization rates of linear polyenes simulated with time-dependent configuration interaction with an absorbing potential," *J. Chem. Phys.* **141**, 174104 (2014).
- 10 P. Krause, J. A. Sonk, and H. B. Schlegel, "Strong field ionization rates simulated with time-dependent configuration interaction and an absorbing potential," *J. Chem. Phys.* **140**, 174113 (2014).
- 11 P. Krause and H. B. Schlegel, "Angle-dependent ionization of hydrides AH_n calculated by time-dependent configuration interaction with an absorbing potential," *J. Phys. Chem. A* **119**, 10212 (2015).
- 12 P. Krause and H. B. Schlegel, "Angle-dependent ionization of small molecules by time-dependent configuration interaction and an absorbing potential," *J. Phys. Chem. Lett.* **6**, 2140 (2015).
- 13 Q. Liao, W. Li, and H. B. Schlegel, "Angle-dependent strong-field ionization of triple bonded systems calculated by time-dependent configuration interaction with an absorbing potential," *Can. J. Chem.* **94**, 989 (2016).
- 14 P. Hoerner and H. B. Schlegel, "Angular dependence of ionization of CH_3X using time-dependent configuration interaction with an absorbing potential," *J. Phys. Chem. A* **121**, 5940 (2017).
- 15 P. Hoerner and H. B. Schlegel, "Angular dependence of ionization by circularly polarized light calculated with time-dependent configuration interaction with an absorbing potential," *J. Phys. Chem. A* **121**, 1336 (2017).
- 16 P. Hoerner and H. B. Schlegel, "Angular dependence of strong field ionization of haloacetylenes, $HCCX$ ($X = F, Cl, Br, I$) using time-dependent configuration interaction with an absorbing potential," *J. Phys. Chem. C* **122**, 13751 (2018).
- 17 P. Hoerner, M. K. Lee, and H. B. Schlegel, "Angular dependence of strong field ionization of N_2 by time-dependent configuration interaction using density functional theory and the Tamm-Dancoff approximation," *J. Chem. Phys.* **151**, 054102 (2019).
- 18 J. G. Muga, J. P. Palao, B. Navarro, and I. L. Egusquiza, "Complex absorbing potentials," *Phys. Rep.* **395**, 357 (2004).
- 19 K. L. Ishikawa and T. Sato, "A review on *ab initio* approaches for multielectron dynamics," *IEEE J. Sel. Top. Quantum Electron.* **21**, 8700916 (2015).
- 20 K. Hino, T. Ishihara, F. Shimizu, N. Toshima, and J. H. McGuire, "Double photoionization of helium using many-body perturbation-theory," *Phys. Rev. A* **48**, 1271 (1993).
- 21 A. Becker and F. H. M. Faisal, "Mechanism of laser-induced double ionization of helium," *J. Phys. B: At., Mol. Opt. Phys.* **29**, L197 (1996).
- 22 A. Becker and F. H. M. Faisal, "Interplay of electron correlation and intense field dynamics in the double ionization of helium," *Phys. Rev. A* **59**, R1742 (1999).
- 23 D. Dundas, K. T. Taylor, J. S. Parker, and E. S. Smyth, "Double-ionization dynamics of laser-driven helium," *J. Phys. B: At., Mol. Opt. Phys.* **32**, L231 (1999).
- 24 K. Harumiya, I. Kawata, H. Kono, and Y. Fujimura, "Exact two-electron wave packet dynamics of H_2 in an intense laser field: Formation of localized ionic states H^+H^- ," *J. Chem. Phys.* **113**, 8953 (2000).
- 25 M. Lein, E. K. U. Gross, and V. Engel, "Intense-field double ionization of helium: Identifying the mechanism," *Phys. Rev. Lett.* **85**, 4707 (2000).
- 26 A. Becker and F. H. M. Faisal, "S-matrix analysis of coincident measurement of two-electron energy distribution for double ionization of He in an intense laser field," *Phys. Rev. Lett.* **89**, 193003 (2002).
- 27 G. L. Kamta and A. F. Starace, "Multielectron system in an ultrashort, intense laser field: A nonperturbative, time-dependent two-active-electron approach," *Phys. Rev. A* **65**, 053418 (2002).
- 28 M. Lein, T. Kreibich, E. K. U. Gross, and V. Engel, "Strong-field ionization dynamics of a model H_2 molecule," *Phys. Rev. A* **65**, 033403 (2002).
- 29 P. Selles, L. Malegat, and A. K. Kazansky, "Ab initio calculation of the whole set of He double-photoionization cross sections," *Phys. Rev. A* **65**, 032711 (2002).
- 30 J. Colgan, M. S. Pindzola, and F. Robicheaux, "Time-dependent close-coupling calculations for the double photoionization of He and H_2 ," *J. Phys. B: At., Mol. Opt. Phys.* **37**, L377 (2004).
- 31 C. F. D. Faria, H. Schomerus, X. Liu, and W. Becker, "Electron-electron dynamics in laser-induced nonsequential double ionization," *Phys. Rev. A* **69**, 043405 (2004).
- 32 T. Kato and H. Kono, "Time-dependent multiconfiguration theory for electronic dynamics of molecules in an intense laser field," *Chem. Phys. Lett.* **392**, 533 (2004).
- 33 E. Fomouou, G. L. Kamta, G. Edah, and B. Piroux, "Theory of multiphoton single and double ionization of two-electron atomic systems driven by short-wavelength electric fields: An *ab initio* treatment," *Phys. Rev. A* **74**, 063409 (2006).
- 34 C. Ruiz, L. Plaja, L. Roso, and A. Becker, "Ab initio calculation of the double ionization of helium in a few-cycle laser pulse beyond the one-dimensional approximation," *Phys. Rev. Lett.* **96**, 053001 (2006).
- 35 L. A. A. Nikolopoulos and P. Lambropoulos, "Time-dependent theory of double ionization of helium under XUV radiation," *J. Phys. B: At., Mol. Opt. Phys.* **40**, 1347 (2007).
- 36 E. Dehghanian, A. D. Bandrauk, and G. L. Kamta, "Enhanced ionization of the H_2 molecule driven by intense ultrashort laser pulses," *Phys. Rev. A* **81**, 061403 (2010).
- 37 R. Nepstad, T. Birkeland, and M. Forre, "Numerical study of two-photon ionization of helium using an *ab initio* numerical framework," *Phys. Rev. A* **81**, 063402 (2010).

- ³⁸E. Dehghanian, A. D. Bandrauk, and G. L. Kamta, "Enhanced ionization of the non-symmetric HeH⁺ molecule driven by intense ultrashort laser pulses," *J. Chem. Phys.* **139**, 084315 (2013).
- ³⁹M. Brics, J. Rapp, and D. Bauer, "Nonsequential double ionization with time-dependent renormalized-natural-orbital theory," *Phys. Rev. A* **90**, 053418 (2014).
- ⁴⁰P. Wustelt, M. Moller, M. S. Schoffler, X. H. Xie, V. Hanus, A. M. Saylor, A. Baltuska, G. G. Paulus, and M. Kitzler, "Numerical investigation of the sequential-double-ionization dynamics of helium in different few-cycle-laser-field shapes," *Phys. Rev. A* **95**, 023411 (2017).
- ⁴¹A. A. Golubeva, P. A. Pieniasek, and A. I. Krylov, "A new electronic structure method for doublet states: Configuration interaction in the space of ionized $1h$ and $2h1p$ determinants," *J. Chem. Phys.* **130**, 124113 (2009).
- ⁴²A. Fleischer *et al.*, "Probing angular correlations in sequential double ionization," *Phys. Rev. Lett.* **107**, 113003 (2011).
- ⁴³A. N. Pfeiffer, S. G. Sayres, and S. R. Leone, "Calculation of valence electron motion induced by sequential strong-field ionisation," *Mol. Phys.* **111**, 2283 (2013).
- ⁴⁴M. Abu-samha and L. B. Madsen, "Interrogation of orbital structure by elliptically polarized intense femtosecond laser pulses," *Phys. Rev. A* **84**, 023411 (2011).
- ⁴⁵H. J. Worner and P. B. Corkum, "Imaging and controlling multielectron dynamics by laser-induced tunnel ionization," *J. Phys. B* **44**, 041001 (2011).
- ⁴⁶M. Murakami, G. P. Zhang, and S. I. Chu, "Multielectron effects in the photoelectron momentum distribution of noble-gas atoms driven by visible-to-infrared-frequency laser pulses: A time-dependent density-functional-theory approach," *Phys. Rev. A* **95**, 053419 (2017).
- ⁴⁷H. Hasegawa, Y. Ikeda, K. Sonoda, T. Sato, A. Iwasaki, and K. Yamanouchi, "Angular dependence of ionization probability of C₂H₂ in a linearly polarized intense laser field," *Chem. Phys. Lett.* **662**, 235 (2016).
- ⁴⁸X. Xie *et al.*, "Selective control over fragmentation reactions in polyatomic molecules using impulsive laser alignment," *Phys. Rev. Lett.* **112**, 163003 (2014).
- ⁴⁹M. Suzuki, "General decomposition-theory of ordered exponentials," *Proc. Jpn. Acad., Ser. B* **69**, 161 (1993).
- ⁵⁰T. H. Dunning, "Gaussian-basis sets for use in correlated molecular calculations. I. The atoms boron through neon and hydrogen," *J. Chem. Phys.* **90**, 1007 (1989).
- ⁵¹M. J. Frisch, G. W. Trucks, H. B. Schlegel, G. E. Scuseria *et al.*, Gaussian Development Version, Revision J.02, Wallingford, CT, 2010.
- ⁵²NIST Chemistry WebBook; accessed October 2019.
- ⁵³R. I. Hall, G. Dawber, K. Ellis, M. Zubek, L. Avaldi, and G. C. King, "Near-threshold study of the neon photoelectron satellites," *J. Phys. B: At., Mol. opt. Phys.* **24**, 4133 (1991).
- ⁵⁴R. I. Hall, K. Ellis, A. McConkey, G. Dawber, L. Avaldi, M. A. Macdonald, and G. C. King, "Double and single ionization of neon, argon and krypton in the threshold region studied by photoelectron ion coincidence spectroscopy," *J. Phys. B: At., Mol. Opt. Phys.* **25**, 377 (1992).
- ⁵⁵J. R. Appling, B. E. Jones, L. E. Abbey, D. E. Bostwick, and T. F. Moran, "Doubly charged ion mass-spectra. 7—Acetylenes," *Org. Mass Spectrom.* **18**, 282 (1983).
- ⁵⁶S. R. Andrews, F. M. Harris, and D. E. Parry, "A combined experimental and theoretical investigation of C₂H₂²⁺ electronic-state energies," *Chem. Phys.* **166**, 69 (1992).
- ⁵⁷O. Furuhashi, T. Kinugawa, S. Masuda, C. Yamada, and S. Ohtani, "Double charge transfer spectroscopy of acetylene dication C₂H₂²⁺ at vibrational resolution," *Chem. Phys. Lett.* **342**, 625 (2001).